

Hole subband dispersions in a cylindrical Ge nanowire: exact solution of the axial Luttinger-Kohn effective mass model

Rui Li (李睿) ^{1,*}

¹*Key Laboratory for Microstructural Material Physics of Hebei Province,
School of Science, Yanshan University, Qinhuangdao 066004, China*

(Dated: November 8, 2023)

Based on the Luttinger-Kohn Hamiltonian in the axial approximation, the transcendental equation determining the hole subband dispersions in a cylindrical Ge nanowire is analytically derived. This equation is more general than that derived using the spherical approximation, and is suitable to study the growth direction dependence of the subband dispersions. The axial approximation almost gives the accurate low-energy subband dispersions for high symmetry nanowire growth directions [001] and [111]. The perturbation corrections from the non-axial terms are negligible for these two directions. The lowest two subband dispersions can be regarded as two shifted parabolic curves with an energy gap at $k_z = 0$ for both growth directions [001] and [111]. At the site of the energy gap, the eigenstates for growth direction [111] are inverted types of that for growth direction [001]. A nanowire growth direction where the energy gap at $k_z = 0$ closes is predicted to exist between directions [001] and [111].

I. INTRODUCTION

Holes in low dimensional semiconductor nanostructures have attracted considerable interests for decades [1–9]. The early investigations mainly focused on the quasi two-dimensional (2D) hole systems, such as semiconductor quantum wells and heterostructures [2–4, 10]. The effective mass, the subband dispersions, and the spin splitting induced by bulk or structure inversion asymmetries have been extensively studied [2, 11–13]. The anisotropic and nonparabolic behaviours of the hole dispersions are revealed [3, 14, 15], and the Rashba spin splitting is shown to be cubic in momentum [13, 16].

Quasi one-dimensional (1D) hole systems, on the other hand, is relatively less studied. Recently, quasi-1D hole gas was experimentally realized in a Ge/Si core/shell nanowire heterostructures [17], and subsequent experiments revealed a possible strong hole spin-orbit coupling in such system [18–20]. A strong linear in momentum spin-orbit coupling was demonstrated theoretically in the presence of a strong electric field [21–23] or a strong magnetic field [24, 25]. The potential strong spin-orbit coupling has stimulated a series of studies in quasi-1D hole systems, such as the using of hole spins in nanowire quantum dots as quantum information carriers [26–31], and the searching of Majorana fermions by placing the 1D hole gas in proximity to an s-wave superconductor [32, 33].

The bulk hole states of semiconductor Ge are described by the 4×4 Luttinger-Kohn Hamiltonian [34, 35]. It is possible to have an exact solution to the effective mass model for a quasi-2D hole system, e.g., quantum well [4]. However, as far as we know, it is impossible for quasi-1D hole systems unless approximations are made to the Luttinger-Kohn Hamiltonian. The subband dispersions

can be exactly solved in a cylindrical nanowire by using the Luttinger-Kohn Hamiltonian in the spherical approximation [6, 7]. However, the spherical approximation fails to account for the growth direction dependence of the subband dispersions. A more reasonable approximation is the axial approximation [11, 16, 36]. Also, for quasi-2D hole systems, the axial approximation is shown to be most accurate for the high-symmetry growth directions [001] and [111] [16].

Here, we extend the exact solvability of the hole subband problem in a cylindrical Ge nanowire from the spherical approximation to the axial approximation. We analytically derive a transcendental equation, whose solutions give the hole subband dispersions in the nanowire. The axial approximation is almost accurate for high-symmetry nanowire growth directions [001] and [111]. For example, the first nonvanishing energy correction to the lowest subband dispersion $|F_z| = 1/2$ comes from perturbation coupling to the much higher subband dispersion $|F_z| = 5/2$ (for direction [111]) and $|F_z| = 7/2$ (for direction [001]). The lowest two subband dispersions can be regarded as two shifted parabolic curves with an energy gap at $k_z = 0$ for both of the high symmetry directions. However, the lowest two eigenstates at $k_z = 0$ for growth direction [111] are inverted forms of that for growth direction [001]. We then predict there exists a gap closing site when the growth direction is rotated from [001] to [111]. Calculations based on the axial approximation confirm this critical growth direction at $\theta \approx 38.258^\circ$ and $\phi = 45^\circ$.

II. EFFECTIVE MASS MODEL OF THE HOLE GAS

We consider a quasi-1D hole gas in a cylindrical Ge nanowire. The hole gas can move freely in the longitudinal direction while is strongly confined in the trans-

* ruili@ysu.edu.cn

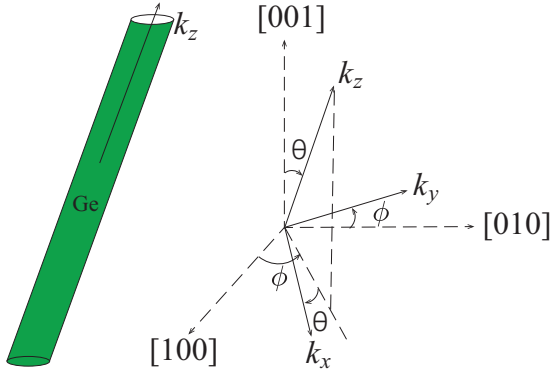


FIG. 1. A cylindrical Ge nanowire grown along the crystal direction (θ, ϕ) is under investigation. The nanowire axis is defined as the k_z axis, and the orientations of the coordinate axes $k_{x,y,z}$ relative to the crystal cubic axes are described by two angles θ and ϕ . Note that the k_y axis is in the $[100]$ - $[010]$ plane.

verse direction of the nanowire. The strong transverse confinement leads to the subband quantization of the hole gas [6, 7, 37, 38]. For semiconductor Ge, the spin-orbit split-off band is 297 meV far away from the top most valence band [39], such that the bulk hole states are well described by the 4×4 Luttinger-Kohn Hamiltonian [35]. Here, in order to study the hole subband dispersions in nanowires grown along various crystal directions, we adopt the Luttinger-Kohn Hamiltonian in the axial approximation instead of the frequently used spherical approximation [21, 40]. The Luttinger-Kohn Hamiltonian in the axial approximation reads [16]

$$H_{\text{LK}}^{\text{axial}} = \frac{\hbar^2}{2m} \begin{pmatrix} F & H & I & 0 \\ H^* & G & 0 & I \\ I^* & 0 & G & -H \\ 0 & I^* & -H^* & F \end{pmatrix}, \quad (1)$$

where m is the free electron mass and

$$\begin{aligned} F &= (\gamma_1 + \tilde{\gamma}_1)(k_x^2 + k_y^2) + (\gamma_1 - 2\tilde{\gamma}_1)k_z^2, \\ G &= (\gamma_1 - \tilde{\gamma}_1)(k_x^2 + k_y^2) + (\gamma_1 + 2\tilde{\gamma}_1)k_z^2, \\ H &= -2\sqrt{3}\tilde{\gamma}_2 k_x k_y, \\ I &= -\sqrt{3}\tilde{\gamma}_3 k_x^2, \end{aligned} \quad (2)$$

with $k_{\pm} = k_x \pm ik_y$ and

$$\begin{aligned} \tilde{\gamma}_1 &= (1 - \zeta)\gamma_2 + \zeta\gamma_3, \\ \tilde{\gamma}_2 &= \frac{2}{3}\zeta\gamma_2 + (1 - \frac{2}{3}\zeta)\gamma_3, \\ \tilde{\gamma}_3 &= \frac{1}{6}(3 - \zeta)\gamma_2 + \frac{1}{6}(3 + \zeta)\gamma_3. \end{aligned} \quad (3)$$

Here $\zeta = \sin^2 \theta [3 - (3/8)(7 + \cos 4\phi) \sin^2 \theta]$, where θ is the azimuthal angle and ϕ is the polar angle of the nanowire axis with respect to the $[001]$ direction (see Fig. 1) [16], and $\gamma_1 = 13.35$, $\gamma_2 = 4.25$, and $\gamma_3 = 5.69$ are the Luttinger parameters for semiconductor Ge [41].

We use an infinite cylindrical well to model the transverse confining potential of the hole gas, such that the effective mass Hamiltonian of the hole gas reads

$$H = H_{\text{LK}}^{\text{axial}} + V(r), \quad (4)$$

where

$$V(r) = \begin{cases} 0, & r < R, \\ \infty, & r > R, \end{cases} \quad (5)$$

with $r = \sqrt{x^2 + y^2}$ and R being the radius of the Ge nanowire. We note that in the effective mass model (4), the replacements $k_{x,y} = -i\partial_{x,y}$ should be made. Interestingly, Hamiltonian H commutes with the total angular momentum $F_z = -i\partial_\varphi + J_z$, where $\varphi = \arctan(x/y)$ and J_z is the z component of the standard spin $3/2$ matrices [16]. Hence, Hamiltonian H and operator F_z have common eigenstates. This is the key to the exact solution of the effective mass model (4) of the hole gas.

Although we adopt the Luttinger-Kohn Hamiltonian in the axial approximation in our calculations, in the following we will show that the axial approximation is indeed an excellent approximation for the high-symmetry nanowire growth directions $[001]$ ($\theta = 0^\circ$ and $\phi = 0^\circ$) and $[111]$ ($\theta = \arccos(1/\sqrt{3})$ and $\phi = 45^\circ$). This assertion is also well known in the quasi-2D hole subband calculations, where the growth directions refer to a quantum well [16].

III. THE TRANSCENDENTAL EQUATION

For a fixed k_z value, we want to solve both the eigenvalues and the corresponding eigenfunctions of Hamiltonian (4). Due to the conservation of the total angular momentum F_z [16], the eigenfunctions can be classified by $F_z = m + 1/2$, with m being an integer. Inside the well $r < R$, the confining potential is zero, Hamiltonian H is reduced to the bulk Hamiltonian $H_{\text{LK}}^{\text{axial}}$. Therefore, our first step is to obtain the bulk spectrum and the corresponding bulk wavefunctions, i.e., the common eigenfunctions of $H_{\text{LK}}^{\text{axial}}$ and F_z . Then, we expand the eigenfunction in terms of the bulk wavefunctions by introducing a series of coefficients. At last, letting the eigenfunction satisfy the desired hard wall boundary condition, we are able to obtain an equation array for the coefficients. Solving this equation array leads to the exact solution of the effective mass model (4).

The bulk spectrum and the corresponding bulk wavefunctions can be obtained by solving $H_{\text{LK}}^{\text{axial}}\Psi_b(r, \varphi, z) = E\Psi_b(r, \varphi, z)$ in the cylindrical coordinate system where $x = r \cos \varphi$, $y = r \sin \varphi$, and $z = z$. The detailed derivations are given in the appendix A, we have two branches of bulk spectrum

$$E = \frac{\hbar^2}{2m} [\gamma_1(\mu^2 + k_z^2) \pm X_\mu], \quad (6)$$

where

$$X_\mu = \sqrt{\tilde{\gamma}_1^2(\mu^2 - 2k_z^2)^2 + 3\mu^2(4\tilde{\gamma}_2^2k_z^2 + \tilde{\gamma}_3^2\mu^2)}, \quad (7)$$

with $\mu^2 = k_x^2 + k_y^2$. For each branch of bulk spectrum, there exist two bulk wavefunctions whose explicit forms are also given in the appendix A.

$$\begin{aligned} \Psi_1(r) &= \left(c_1 \frac{2i\tilde{\gamma}_2k_z}{\tilde{\gamma}_3\mu_1} + c_2 \frac{\tilde{\gamma}_1(\mu_1^2 - 2k_z^2) + X_{\mu_1}}{\sqrt{3}\tilde{\gamma}_3\mu_1^2} \right) J_{m-1}(\mu_1 r) + \left(c_3 \frac{2i\tilde{\gamma}_2k_z}{\tilde{\gamma}_3\mu_2} + c_4 \frac{\tilde{\gamma}_1(\mu_2^2 - 2k_z^2) - X_{\mu_2}}{\sqrt{3}\tilde{\gamma}_3\mu_2^2} \right) J_{m-1}(\mu_2 r), \\ \Psi_2(r) &= \left(c_1 \frac{-\tilde{\gamma}_1(\mu_1^2 - 2k_z^2) + X_{\mu_1}}{\sqrt{3}\tilde{\gamma}_3\mu_1^2} - c_2 \frac{2i\tilde{\gamma}_2k_z}{\tilde{\gamma}_3\mu_1} \right) J_m(\mu_1 r) + \left(c_3 \frac{-\tilde{\gamma}_1(\mu_2^2 - 2k_z^2) - X_{\mu_2}}{\sqrt{3}\tilde{\gamma}_3\mu_2^2} - c_4 \frac{2i\tilde{\gamma}_2k_z}{\tilde{\gamma}_3\mu_2} \right) J_m(\mu_2 r), \\ \Psi_3(r) &= c_2 J_{m+1}(\mu_1 r) + c_4 J_{m+1}(\mu_2 r), \\ \Psi_4(r) &= c_1 J_{m+2}(\mu_1 r) + c_3 J_{m+2}(\mu_2 r), \end{aligned} \quad (9)$$

with $J_m(\mu r)$ being the m -order Bessel function [42], and

$$\mu_{1,2} = \left(\frac{-b \mp \sqrt{b^2 - 4ac}}{2a} \right)^{1/2}, \quad (10)$$

with

$$\begin{aligned} a &= \gamma_1^2 - \tilde{\gamma}_1^2 - 3\tilde{\gamma}_3^2, \\ b &= 2[\gamma_1^2k_z^2 + 2(\tilde{\gamma}_1^2 - 3\tilde{\gamma}_2^2)k_z^2 - 2\gamma_1mE/\hbar^2], \\ c &= \gamma_1^2k_z^4 - 4\tilde{\gamma}_1^2k_z^4 - 4\gamma_1k_z^2mE/\hbar^2 + 4m^2E^2/\hbar^4. \end{aligned} \quad (11)$$

$$\begin{vmatrix} \frac{2i\tilde{\gamma}_2k_z}{\tilde{\gamma}_3\mu_1} J_{m-1}(\mu_1 R) & \frac{\tilde{\gamma}_1(\mu_1^2 - 2k_z^2) + X_{\mu_1}}{\sqrt{3}\tilde{\gamma}_3\mu_1^2} J_{m-1}(\mu_1 R) & \frac{2i\tilde{\gamma}_2k_z}{\tilde{\gamma}_3\mu_2} J_{m-1}(\mu_2 R) & \frac{\tilde{\gamma}_1(\mu_2^2 - 2k_z^2) - X_{\mu_2}}{\sqrt{3}\tilde{\gamma}_3\mu_2^2} J_{m-1}(\mu_2 R) \\ \frac{-\tilde{\gamma}_1(\mu_1^2 - 2k_z^2) + X_{\mu_1}}{\sqrt{3}\tilde{\gamma}_3\mu_1^2} J_m(\mu_1 R) & -\frac{2i\tilde{\gamma}_2k_z}{\tilde{\gamma}_3\mu_1} J_m(\mu_1 R) & \frac{-\tilde{\gamma}_1(\mu_2^2 - 2k_z^2) - X_{\mu_2}}{\sqrt{3}\tilde{\gamma}_3\mu_2^2} J_m(\mu_2 R) & -\frac{2i\tilde{\gamma}_2k_z}{\tilde{\gamma}_3\mu_2} J_m(\mu_2 R) \\ 0 & J_{m+1}(\mu_1 R) & 0 & J_{m+1}(\mu_2 R) \\ J_{m+2}(\mu_1 R) & 0 & J_{m+2}(\mu_2 R) & 0 \end{vmatrix} = 0. \quad (12)$$

This equation is an implicit equation of the energy eigenvalue E . By fixing the total angular momentum $F_z = m + 1/2$, i.e., fixing m , for a given k_z value, we can solve a series of energies satisfying Eq. (12). When the energies are plotted as a function of k_z , we have the subband dispersions of the hole gas. Once an eigenvalue E is solved from Eq. (12), we can solve the coefficients $c_{1,2,3,4}$ from the matrix equation (see appendix B), in combination with the normalization condition of the eigenfunction [43]. The two components $\Psi_{1,3}(r)$ of the eigenfunction $\Psi(r, \varphi, z)$ can be chosen as imaginary, while the other two components $\Psi_{2,4}(r)$ can be chosen as real.

We note that from symmetry analysis [43], the hole energies are two-fold degenerate, i.e., spin degenerate. If

The eigenfunction of Hamiltonian (4) can now be expanded in terms of the four bulk wave functions, i.e.,

$$\Psi(r, \varphi, z) \equiv \begin{pmatrix} \Psi_1(r)e^{i(m-1)\varphi} \\ \Psi_2(r)e^{im\varphi} \\ \Psi_3(r)e^{i(m+1)\varphi} \\ \Psi_4(r)e^{i(m+2)\varphi} \end{pmatrix} e^{ik_z z}, \quad (8)$$

where

Here $\mu_{1,2}$ are obtained by inversely solving Eq. (6). For a given energy E , it crosses the positive branch dispersion [the '+' branch of Eq. (6)] at the site μ_1 , and it crosses the minus branch dispersion [the '-' branch of Eq. (6)] at the site μ_2 . It is evident that $\mu_1 < \mu_2$, just as indicated in Eq. (10).

Imposing the hard-wall boundary condition to the eigenfunction $\Psi(R, \varphi, z) = 0$, we obtain four equations of the expansion coefficients $c_{1,2,3,4}$ (for details see appendix B). The determinant of the coefficient matrix must be zero, such that we have the following transcendental equation

Eq. (8) is an eigenfunction with eigenvalue $E(k_z)$, then the same is the following eigenfunction

$$\begin{pmatrix} \Psi_4^*(r)e^{-i(m+2)\varphi} \\ \Psi_3^*(r)e^{-i(m+1)\varphi} \\ \Psi_2^*(r)e^{-im\varphi} \\ \Psi_1^*(r)e^{-i(m-1)\varphi} \end{pmatrix} e^{ik_z z}. \quad (13)$$

Eigenfunction (13) corresponds to a total angular momentum $F_z = -(m + 1/2)$. Hence, combining Eqs. (8) and (13), the hole spin degeneracy can be simply written as $|F_z| = m + 1/2$, with $m = 0, 1, 2, \dots$

A. The case $k_z = 0$

We discuss here the subband energies and the corresponding eigenfunctions at the special wave vector site $k_z = 0$ [40]. When $k_z = 0$, the transcendental equation (12) can be reduced to two independent equations, one reads

$$\frac{\sqrt{\tilde{\gamma}_1^2 + 3\tilde{\gamma}_3^2} + \tilde{\gamma}_1}{\sqrt{\tilde{\gamma}_1^2 + 3\tilde{\gamma}_3^2} - \tilde{\gamma}_1} J_{m-1}(\mu_1 R) J_{m+1}(\mu_2 R) + J_{m-1}(\mu_2 R) J_{m+1}(\mu_1 R) = 0, \quad (14)$$

and the other reads

$$\frac{\sqrt{\tilde{\gamma}_1^2 + 3\tilde{\gamma}_3^2} + \tilde{\gamma}_1}{\sqrt{\tilde{\gamma}_1^2 + 3\tilde{\gamma}_3^2} - \tilde{\gamma}_1} J_m(\mu_2 R) J_{m+2}(\mu_1 R) + J_m(\mu_1 R) J_{m+2}(\mu_2 R) = 0. \quad (15)$$

If the energy eigenvalue E is solved from Eq. (14), we are easy to find a simple solution for the expansion coefficients

$$c_2 = iJ_{m+1}(\mu_2 R), \quad c_4 = -iJ_{m+1}(\mu_1 R), \quad c_1 = c_3 = 0. \quad (16)$$

This result indicates that two components of the eigenfunction [see Eq. (9)] are zero, i.e., $\Psi_2(r) = \Psi_4(r) = 0$. If the energy eigenvalue E is solved from Eq. (15), the expansion coefficients of the eigenfunction can be solved as

$$c_1 = J_{m+2}(\mu_2 R), \quad c_3 = -J_{m+2}(\mu_1 R), \quad c_2 = c_4 = 0. \quad (17)$$

This result indicates that the following two components $\Psi_1(r)$ and $\Psi_3(r)$ of the eigenfunction are zero instead.

Hence, at the site $k_z = 0$, the eigenfunctions always have two vanishing components, i.e., either $\Psi_{1,3}(r)$ or $\Psi_{2,4}(r)$ are zero [21, 40, 43]. We also note that by choosing the simple solutions as Eqs. (16) and (17), the eigenfunctions are not normalized.

B. The case $\tilde{\gamma}_1 = \tilde{\gamma}_2 = \tilde{\gamma}_3$

Here, we temporarily ignore the expressions of $\tilde{\gamma}_{1,2,3}$ given in Eq. (3), and consider the ideal case where $\tilde{\gamma}_1 = \tilde{\gamma}_2 = \tilde{\gamma}_3 = \gamma_s$. In this case, the Luttinger-Kohn Hamiltonian in the axial approximation H_{LK}^{axial} is reduced to that in the spherical approximation. The formulas based on the spherical approximation in calculating the hole subband dispersions are well established in literatures [7].

Now, the parameter X_μ defined in Eq. (7) can be simplified to

$$X_\mu = 2\gamma_s(\mu^2 + k_z^2), \quad (18)$$

and the $\mu_{1,2}$ given in Eq. (10) can be simplified to

$$\mu_{1,2} = \sqrt{\frac{2mE}{(\gamma_1 \pm 2\gamma_s)\hbar^2} - k_z^2}. \quad (19)$$

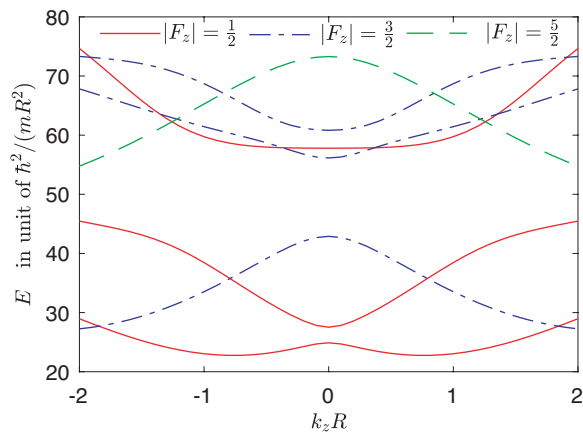


FIG. 2. Hole subband dispersions for growth direction [001]. For a moderate nanowire radius $R = 10$ nm, the energy unit is $\hbar^2/(mR^2) \approx 0.763$ meV. The energy gap of the lowest two subband dispersions at the anticrossing site $k_z R = 0$ is about $2.63\hbar^2/(mR^2)$. The subband minima are located at $k_z R \approx \pm 0.76$. Each dispersion line is two-fold degenerate, i.e., spin degeneracy.

Substituting these results into the transcendental equation Eq. (12), we recover the well-known transcendental equation given by Sercel and Vahala [7]. Also, the two independent transcendental equations (14) and (15) at $k_z = 0$ can be reduced to that given previously [21, 40].

IV. SUBBAND DISPERSIONS AND SUBBAND WAVEFUNCTIONS

A. The results for growth direction [001]

When the growth direction of the Ge nanowire is along the [001] crystal axis, i.e., $k_x \parallel [100]$, $k_y \parallel [010]$, and $k_z \parallel [001]$, the parameters $\tilde{\gamma}_{1,2,3}$ in the Luttinger-Kohn Hamiltonian in the axial approximation read $\tilde{\gamma}_1 = \gamma_2$, $\tilde{\gamma}_2 = \gamma_3$, and $\tilde{\gamma}_3 = (\gamma_2 + \gamma_3)/2$ [15]. Substituting these parameter values into Eq. (12), we can solve the hole subband dispersions for this growth direction.

The hole subband dispersions for growth direction [001] are shown in Fig. 2. Each line in the figure is two-fold degenerate, i.e., spin degenerate. The lowest two subband dispersions, i.e., the lowest two solid lines of $|F_z| = 1/2$, can be regarded as two shifted parabolic curves with an anticrossing at $k_z R = 0$ [24, 25, 44]. The energy gap at the anticrossing site $k_z R = 0$ is about $2.63\hbar^2/(mR^2)$. The subband minima are located at $k_z R \approx \pm 0.76$. We note that the lowest three subband dispersions in Fig. 2 agree well with that obtained previously using the perturbation method [44].

The functional forms of the subband wavefunctions are shown in Fig. 3. At the center of the wave vector space $k_z R = 0$, the wavefunctions always have two non-zero components. Figures 3(a), (b) and (c) show the results at $k_z R = 0$ for the ground, the first excited, and the sec-

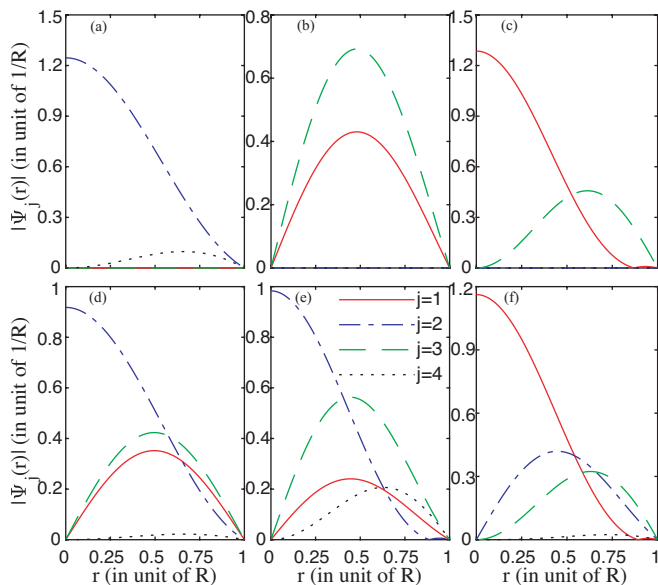


FIG. 3. Hole subband wavefunctions for growth direction [001]. The four components $\Psi_{1,2,3,4}(r)$ of the wavefunction Eq. (8) as a function of the coordinate r . The ground (a), the first excited (b), and the second excited (c) states at $k_z R = 0$. The ground (d), the first excited (e), and the second excited (f) states at $k_z R = 0.8$. Here, we only consider eigenfunctions with positive total angular momentum $F_z > 0$.

ond excited states, respectively. Here the ground state has components $\Psi_{2,4}(r) \neq 0$ and the first excited state has components $\Psi_{1,3}(r) \neq 0$. At the site $k_z R = 0.8$, all the four components of the eigenfunction are nonzero, see the results of the ground, the first excited, and the second excited states in Figs. 3(d), (e) and (f), respectively. Here we only show the eigenfunctions with positive total angular momentum $F_z > 0$.

B. The results for growth direction [111]

When the growth direction of the Ge nanowire is along the [111] crystal axis, i.e., $k_x \parallel [11\bar{2}]$, $k_y \parallel [\bar{1}10]$, and $k_z \parallel [111]$, the parameters $\tilde{\gamma}_{1,2,3}$ in the Luttinger-Kohn Hamiltonian in the axial approximation read $\tilde{\gamma}_1 = \gamma_3$, $\tilde{\gamma}_2 = (2\gamma_2 + \gamma_3)/3$, and $\tilde{\gamma}_3 = (\gamma_2 + 2\gamma_3)/3$ [45, 46]. Substituting these parameter values into the transcendental equation (12), we can solve the hole subband dispersions for this growth direction.

The subband dispersions for growth direction [111] are shown in Fig. 4. Each dispersion line in the figure is two-fold degenerate, e.g. spin degenerate. The lowest two subband dispersions, i.e., the lowest two solid lines of $|F_z| = 1/2$, can still be regarded as two shifted parabolic curves with an anticrossing at $k_z R = 0$ [24, 25, 44]. The energy gap at the anticrossing site is about $0.61\hbar^2/(mR^2)$, much smaller than that for growth direction [001]. The band minima are located at

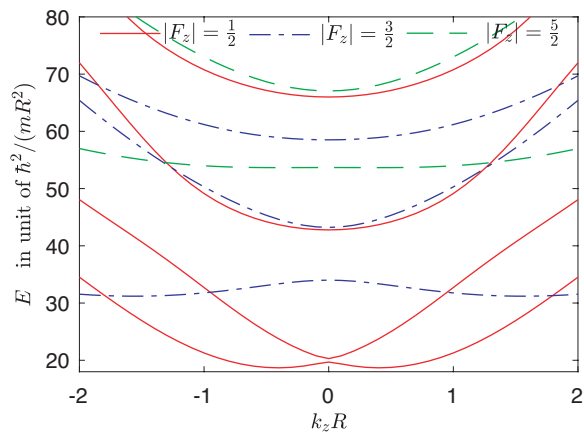


FIG. 4. Hole subband dispersions for growth direction [111]. The energy gap of the lowest two subband dispersions at the anticrossing site $k_z R = 0$ is about $0.61\hbar^2/(mR^2)$. The band minima are located at $k_z R \approx \pm 0.4$. Each dispersion line is two-fold degenerate, i.e., spin degeneracy.

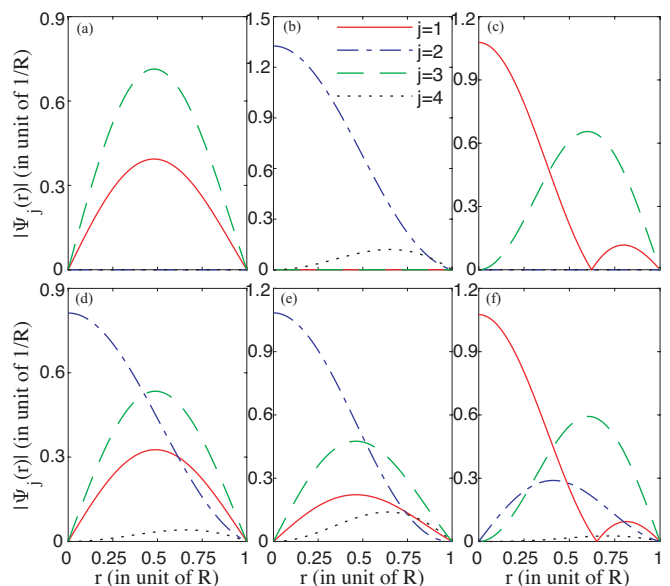


FIG. 5. Hole subband wavefunctions for growth direction [111]. The four components $\Psi_{1,2,3,4}(r)$ of the wavefunctions Eq. (8) as a function of the coordinate r . The ground (a), the first excited (b), and the second excited (c) states at $k_z R = 0$. The ground (d), the first excited (e), and the second excited (f) states at $k_z R = 0.4$. Here, we only consider eigenfunctions with positive total angular momentum $F_z > 0$.

$k_z R \approx \pm 0.40$, also smaller than that for growth direction [001].

The functional forms of the subband wavefunctions are shown in Fig. 5. At $k_z R = 0$, the wavefunction always has two non-zero components. Figures 5(a), (b) and (c) show the functional forms of the ground, the first excited, and the second excited states at $k_z R = 0$, respectively. All the four components of the wavefunction are non-zero at a general site $k_z R \neq 0$. Figures 5(d), (e) and (f) show

the functional form of the ground, the first excited, and the second excited states at the site $k_z R = 0.4$.

Let us focus on the lowest two eigenstates at the anticrossing site $k_z R = 0$, i.e., the site with an energy gap. For the growth direction [111], we have the ground state $\Psi_{1,3}(r) \neq 0$ and the first excited state $\Psi_{2,4}(r) \neq 0$ [see Figs. 5(a) and (b)]. While for the growth direction [001], we have the ground state $\Psi_{2,4}(r) \neq 0$ and the first excited state $\Psi_{2,3}(r) \neq 0$ [see Figs. 3(a) and (b)]. Hence, at the site of the anticrossing, the eigenstates for growth direction [111] are inverted types of that for the growth direction [001]. This result will induce interest consequence we will discuss in Sec. VI.

V. THE EFFECTS OF THE NON-AXIAL TERMS

In this section, we discuss the impacts of the non-axial terms in the general Luttinger-Kohn Hamiltonian on the hole subband dispersions for both growth directions [001] and [111]. For nanowire growth direction [001], the difference between the general Luttinger-Kohn Hamiltonian and that in the axial approximation reads [10, 15]

$$H'_{001} = \frac{\sqrt{3}\hbar^2}{4m}(\gamma_3 - \gamma_2) \begin{pmatrix} 0 & 0 & k_+^2 & 0 \\ 0 & 0 & 0 & k_+^2 \\ k_-^2 & 0 & 0 & 0 \\ 0 & k_-^2 & 0 & 0 \end{pmatrix}. \quad (20)$$

For nanowire growth direction [111], the difference between the general Luttinger-Kohn Hamiltonian and that in the axial approximation reads [45, 46]

$$H'_{111} = -\frac{(\gamma_3 - \gamma_2)\hbar^2}{\sqrt{6}m} \begin{pmatrix} 0 & k_+^2 & 2k_z k_+ & 0 \\ k_-^2 & 0 & 0 & 2k_z k_+ \\ 2k_z k_- & 0 & 0 & -k_+^2 \\ 0 & 2k_z k_- & -k_-^2 & 0 \end{pmatrix}. \quad (21)$$

We now consider H'_{001} or H'_{111} as a perturbation term [47], and discuss its energy corrections to the lowest hole subband dispersion shown in Fig. 2 or 4. The general lowest subband wavefunction of total angular momentum $F_z = 1/2$ can be written as [43]

$$|\Psi_{1/2}\rangle = \begin{pmatrix} \Psi_{I1}(r)e^{-i\varphi} \\ \Psi_{I2}(r) \\ \Psi_{I3}(r)e^{i\varphi} \\ \Psi_{I4}(r)e^{2i\varphi} \end{pmatrix}. \quad (22)$$

Acting the perturbation Hamiltonian H'_{001} on this state, we have (up to a constant factor)

$$H'_{001}|\Psi_{1/2}\rangle \sim \begin{pmatrix} k_+^2 \Psi_{I3}(r)e^{i\varphi} \\ k_+^2 \Psi_{I4}(r)e^{2i\varphi} \\ k_-^2 \Psi_{I1}(r)e^{-i\varphi} \\ k_-^2 \Psi_{I2}(r) \end{pmatrix}. \quad (23)$$

By a simple check of the integral of the angular variable φ in the perturbation matrix element $\langle \Psi_{F_z} | H'_{001} | \Psi_{1/2} \rangle$

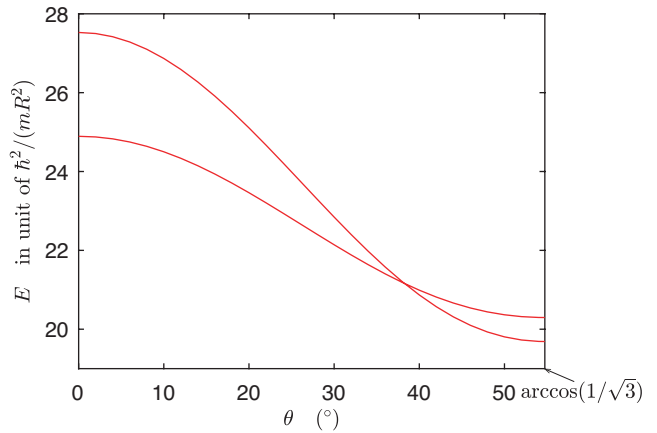


FIG. 6. The lowest two subband energies at $k_z R = 0$ as a function of the nanowire growth direction θ . Here ϕ is fixed at 45° . $\theta = 0^\circ$ corresponds to the growth direction [001] and $\theta = \arccos(1/\sqrt{3})$ corresponds to the growth direction [111]. The energy gap closes at $\theta \approx 38.258^\circ$.

by using $\int_0^{2\pi} d\varphi \exp[i(m - m')\varphi] = \delta_{mm'}$, we find the first non-zero perturbation matrix element comes from subband wavefunction of $|F_z| = 7/2$.

Acting the perturbation Hamiltonian H'_{111} on the state $|\Psi_{1/2}\rangle$, we have (up to a constant factor)

$$H'_{111}|\Psi_{1/2}\rangle \sim \begin{pmatrix} k_+^2 \Psi_{I2}(r) + 2k_z k_+ \Psi_{I3}(r)e^{i\varphi} \\ k_-^2 \Psi_{I1}(r)e^{-i\varphi} + 2k_z k_+ \Psi_{I4}(r)e^{2i\varphi} \\ 2k_z k_- \Psi_{I1}(r)e^{-i\varphi} - k_+^2 \Psi_{I4}(r)e^{2i\varphi} \\ 2k_z k_- \Psi_{I2}(r) - k_-^2 \Psi_{I,3}(r)e^{i\varphi} \end{pmatrix}. \quad (24)$$

By a similar check of the integral of the angular variable φ in $\langle \Psi_{F_z} | H'_{001} | \Psi_{1/2} \rangle$, we find the first non-zero perturbation matrix element comes from the subband wavefunction of $|F_z| = 5/2$.

Therefore, if we are interested only in the low-energy subband dispersions, e.g., the two shifted parabolic curves shown in Figs. 2 and 4, the perturbation contributions from the non-axial terms in the general Luttinger-Kohn Hamiltonian are negligible. Because these two subband dispersions are well separated from those subband dispersions marked with $|F_z| \geq 5/2$ or $|F_z| \geq 7/2$.

VI. THE GAP CLOSURES AT A SPECIAL GROWTH DIRECTION

From the analysis given in Sec. V, we believe the axial approximation indeed reasonably gives both the low-energy subband dispersions and the corresponding subband wavefunctions for both growth directions [001] and [111]. Here, we discuss the possibility of a gap closing at $k_z = 0$ for a special growth direction.

The lowest two eigenstates at $k_z R = 0$ for growth direction [111] are inverted types of that for growth direction [001]. Quantum state inversion has been extensively studied in the field of topological insulator [48, 49], and

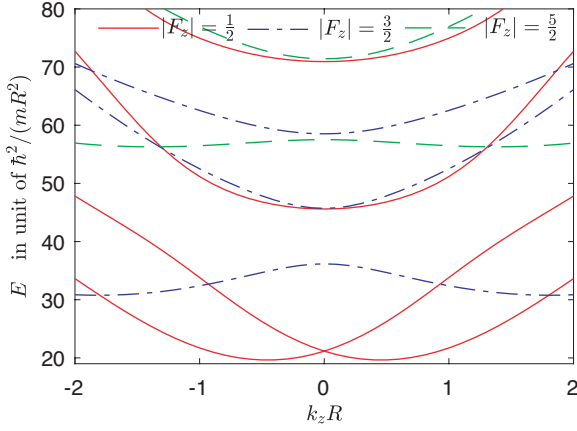


FIG. 7. The hole subband dispersions for the nanowire growth direction $\theta = 38.258^\circ$ and $\phi = 45^\circ$. The subband minima are located at $k_z R = \pm 0.5$. Each dispersion line is two-fold degenerate, i.e., spin degeneracy. There is no energy gap for the lowest two subband dispersions at $k_z R = 0$.

state inversion usually indicates the existence of a gap closing site. Here, we search this gap closing site between nanowire growth directions [001] and [111].

When one angle of the growth direction is fixed at $\phi = 45^\circ$, and the other angle θ is varied from 0° to $\arccos(1/\sqrt{3})$, i.e., from the growth direction [001] to the growth direction [111], the lowest two subband energies at the site $k_z R = 0$ as a function of θ are shown in Fig. 6. We find that there indeed exists a gap closing site at $\theta \approx 38.258^\circ$. Although we obtain this gap closing site by using the Luttinger-Kohn Hamiltonian in the axial approximation, we believe a gap closing site still exists even if the general Luttinger-Kohn Hamiltonian is used.

The hole subband dispersions at the critical growth direction $\theta = 38.258^\circ$ and $\phi = 45^\circ$ are shown in Fig. 7. The lowest two subband dispersions now are two shifted parabolic curves with no energy gap at $k_z R = 0$, i.e., the lowest two parabolic curves cross with each other at $k_z R = 0$. The band minima are located at $k_z R \approx \pm 0.5$.

VII. SUMMARY

We have exactly solved the effective mass model of the hole gas in a cylindrical Ge nanowire, where the Luttinger-Kohn Hamiltonian in the axial approximation is used. A more general transcendental equation beyond the spherical approximation is analytical derived, and the solutions of this equation give the hole subband dispersions in the nanowire. The axial approximation is almost accurate for high symmetry nanowire growth directions [001] and [111]. The lowest two subband dispersions for these two growth directions can be regarded as two shifted parabolic curves with an energy gap the $k_z R = 0$. However, the wavefunctions for growth direction [111] at the gap opening site are inverted types of that for growth direction [001]. Quantum state inversion

at $k_z R = 0$ prompts us to search a gap closing growth direction between [001] and [111]. Calculations based on the axial approximation show this growth direction is located at $\theta \approx 38.258^\circ$ and $\phi = 45^\circ$.

Appendix A: The bulk spectrum and the bulk wavefunctions

The total Hilbert space can be divided into a series of subspaces by considering the conversion of the total angular momentum F_z . The Hilbert subspace labeled with a general total angular momentum $F_z = m + 1/2$ is spanned by $J_{m-1}(\mu r)e^{i(m-1)\varphi}|3/2\rangle$, $J_m(\mu r)e^{im\varphi}|1/2\rangle$, $J_{m+1}(\mu r)e^{i(m+1)\varphi}|-1/2\rangle$, and $J_{m+2}(\mu r)e^{i(m+2)\varphi}|-3/2\rangle$. The bulk Hamiltonian $H_{\text{LK}}^{\text{axial}}$ can be written as a 4×4 matrix in this Hilbert subspace [in unit of $\hbar^2/(2m)$]

$$H_{\text{LK}}^{\text{axial}} = \begin{pmatrix} H_{11} & 2\sqrt{3}i\tilde{\gamma}_2k_z\mu & \sqrt{3}\tilde{\gamma}_3\mu^2 & 0 \\ h.c. & H_{22} & 0 & \sqrt{3}\tilde{\gamma}_3\mu^2 \\ h.c. & 0 & H_{33} & -2\sqrt{3}i\tilde{\gamma}_2k_z\mu \\ 0 & h.c. & h.c. & H_{44} \end{pmatrix}, \quad (\text{A1})$$

where $H_{11} = H_{44} = (\gamma_1 + \tilde{\gamma}_1)\mu^2 + (\gamma_1 - 2\tilde{\gamma}_1)k_z^2$, $H_{22} = H_{33} = (\gamma_1 - \tilde{\gamma}_1)\mu^2 + (\gamma_1 + 2\tilde{\gamma}_1)k_z^2$, and $h.c.$ denotes the Hermitian conjugation. Diagonalizing the matrix (A1), we obtain two branches of bulk spectrum

$$E = \frac{\hbar^2}{2m}[\gamma_1(\mu^2 + k_z^2) \pm X_\mu], \quad (\text{A2})$$

where X_μ is given in Eq. (7). There are two bulk wavefunctions correspond to the ‘+’ branch spectrum

$$\begin{pmatrix} \frac{2i\tilde{\gamma}_2k_z}{\tilde{\gamma}_3\mu} J_{m-1}(\mu r)e^{i(m-1)\varphi} \\ \frac{-\tilde{\gamma}_1(\mu^2 - 2k_z^2) + X_\mu}{\sqrt{3}\tilde{\gamma}_3\mu^2} J_m(\mu r)e^{im\varphi} \\ 0 \\ J_{m+2}(\mu r)e^{i(m+2)\varphi} \end{pmatrix}, \quad (\text{A3})$$

and

$$\begin{pmatrix} \frac{\tilde{\gamma}_1(\mu^2 - 2k_z^2) + X_\mu}{\sqrt{3}\tilde{\gamma}_3\mu^2} J_{m-1}(\mu r)e^{i(m-1)\varphi} \\ -\frac{2i\tilde{\gamma}_2k_z}{\tilde{\gamma}_3\mu} J_m(\mu r)e^{im\varphi} \\ J_{m+1}(\mu r)e^{i(m+1)\varphi} \\ 0 \end{pmatrix}. \quad (\text{A4})$$

There are also two bulk wavefunctions correspond to the ‘-’ branch spectrum

$$\begin{pmatrix} \frac{2i\tilde{\gamma}_2k_z}{\tilde{\gamma}_3\mu} J_{m-1}(\mu r)e^{i(m-1)\varphi} \\ \frac{-\tilde{\gamma}_1(\mu^2 - 2k_z^2) - X_\mu}{\sqrt{3}\tilde{\gamma}_3\mu^2} J_m(\mu r)e^{im\varphi} \\ 0 \\ J_{m+2}(\mu r)e^{i(m+2)\varphi} \end{pmatrix}, \quad (\text{A5})$$

and

$$\begin{pmatrix} \frac{\tilde{\gamma}_1(\mu^2 - 2k_z^2) - X_\mu}{\sqrt{3}\tilde{\gamma}_3\mu^2} J_{m-1}(\mu r)e^{i(m-1)\varphi} \\ -\frac{2i\tilde{\gamma}_2k_z}{\tilde{\gamma}_3\mu} J_m(\mu r)e^{im\varphi} \\ J_{m+1}(\mu r)e^{i(m+1)\varphi} \\ 0 \end{pmatrix}. \quad (\text{A6})$$

Appendix B: The equation array for the coefficients

 $c_{1,2,3,4}$

The hard-wall boundary condition $\Psi(R, \varphi) = 0$ can be written as

$$\begin{aligned}
 \frac{2i\tilde{\gamma}_2k_z}{\tilde{\gamma}_3\mu_1}J_{m-1}(\mu_1R)c_1 + \frac{\tilde{\gamma}_1(\mu_1^2 - 2k_z^2) + X_{\mu_1}}{\sqrt{3}\tilde{\gamma}_3\mu_1^2}J_{m-1}(\mu_1R)c_2 + \frac{2i\tilde{\gamma}_2k_z}{\tilde{\gamma}_3\mu_2}J_{m-1}(\mu_2R)c_3 + \frac{\tilde{\gamma}_1(\mu_2^2 - 2k_z^2) - X_{\mu_2}}{\sqrt{3}\tilde{\gamma}_3\mu_2^2}J_{m-1}(\mu_2R)c_4 &= 0, \\
 \frac{-\tilde{\gamma}_1(\mu_1^2 - 2k_z^2) + X_{\mu_1}}{\sqrt{3}\tilde{\gamma}_3\mu_1^2}J_m(\mu_1R)c_1 - \frac{2i\tilde{\gamma}_2k_z}{\tilde{\gamma}_3\mu_1}J_m(\mu_1R)c_2 - \frac{\tilde{\gamma}_1(\mu_2^2 - 2k_z^2) + X_{\mu_2}}{\sqrt{3}\tilde{\gamma}_3\mu_2^2}J_m(\mu_2R)c_3 - \frac{2i\tilde{\gamma}_2k_z}{\tilde{\gamma}_3\mu_2}J_m(\mu_2R)c_4 &= 0, \\
 J_{m+1}(\mu_1R)c_2 + J_{m+1}(\mu_2R)c_4 &= 0, \\
 J_{m+2}(\mu_1R)c_1 + J_{m+2}(\mu_2R)c_3 &= 0.
 \end{aligned}
 \tag{B1}$$

-
- [1] A. Baldereschi and N. O. Lipari, Spherical model of shallow acceptor states in semiconductors, *Phys. Rev. B* **8**, 2697 (1973).
- [2] D. A. Broido and L. J. Sham, Effective masses of holes at GaAs-AlGaAs heterojunctions, *Phys. Rev. B* **31**, 888 (1985).
- [3] T. Ando, Hole subband at GaAs/AlGaAs heterojunctions and quantum wells, *Journal of the physical society of Japan* **54**, 1528 (1985).
- [4] L. C. Andreani, A. Pasquarello, and F. Bassani, Hole subbands in strained GaAs-Ga_{1-x}Al_xAs quantum wells: Exact solution of the effective-mass equation, *Phys. Rev. B* **36**, 5887 (1987).
- [5] J.-B. Xia, Electronic structures of zero-dimensional quantum wells, *Phys. Rev. B* **40**, 8500 (1989).
- [6] M. Sweeny, J. Xu, and M. Shur, Hole subbands in one-dimensional quantum well wires, *Superlattices and Microstructures* **4**, 623 (1988).
- [7] P. C. Sercel and K. J. Vahala, Analytical formalism for determining quantum-wire and quantum-dot band structure in the multiband envelope-function approximation, *Phys. Rev. B* **42**, 3690 (1990).
- [8] S. L. Chuang, Efficient band-structure calculations of strained quantum wells, *Phys. Rev. B* **43**, 9649 (1991).
- [9] E. Marcellina, A. R. Hamilton, R. Winkler, and D. Culcer, Spin-orbit interactions in inversion-asymmetric two-dimensional hole systems: A variational analysis, *Phys. Rev. B* **95**, 075305 (2017).
- [10] E. Bangert and G. Landwehr, Self-consistent calculations of electric subbands in p-type GaAlAs-GaAs heterojunctions, *Superlattices and Microstructures* **1**, 363 (1985).
- [11] U. Ekenberg and M. Altarelli, Subbands and Landau levels in the two-dimensional hole gas at the GaAs-Al_xGa_{1-x}As interface, *Phys. Rev. B* **32**, 3712 (1985).
- [12] E. Rashba and E. Sherman, Spin-orbital band splitting in symmetric quantum wells, *Physics Letters A* **129**, 175 (1988).
- [13] R. Winkler, Rashba spin splitting in two-dimensional electron and hole systems, *Phys. Rev. B* **62**, 4245 (2000).
- [14] M. Altarelli, U. Ekenberg, and A. Fasolino, Calculations of hole subbands in semiconductor quantum wells and superlattices, *Phys. Rev. B* **32**, 5138 (1985).
- [15] G. Fishman, Hole subbands in strained quantum-well semiconductors in [hhk] directions, *Phys. Rev. B* **52**, 11132 (1995).
- [16] R. Winkler, *Spin-Orbit Coupling Effects in Two-Dimensional Electron and Hole Systems* (Springer, Berlin, 2003).
- [17] W. Lu, J. Xiang, B. P. Timko, Y. Wu, and C. M. Lieber, One-dimensional hole gas in germanium/silicon nanowire heterostructures, *Proceedings of the National Academy of Sciences* **102**, 10046 (2005).
- [18] A. P. Higginbotham, F. Kuemmeth, T. W. Larsen, M. Fitzpatrick, J. Yao, H. Yan, C. M. Lieber, and C. M. Marcus, Antilocalization of coulomb blockade in a Ge/Si nanowire, *Phys. Rev. Lett.* **112**, 216806 (2014).
- [19] F. N. M. Froning, M. J. Rančić, B. Hetényi, S. Bosco, M. K. Rehmann, A. Li, E. P. A. M. Bakkers, F. A. Zwanenburg, D. Loss, D. M. Zumbühl, and F. R. Braakman, Strong spin-orbit interaction and *g*-factor renormalization of hole spins in Ge/Si nanowire quantum dots, *Phys. Rev. Research* **3**, 013081 (2021).
- [20] F. N. M. Froning, L. C. Camenzind, O. A. H. van der Molen, A. Li, E. P. A. M. Bakkers, D. M. Zumbühl, and F. R. Braakman, Ultrafast hole spin qubit with gate-tunable spin-orbit switch functionality, *Nature Nanotechnology* **16**, 308 (2021).
- [21] C. Kloeffel, M. Trif, and D. Loss, Strong spin-orbit interaction and helical hole states in Ge/Si nanowires, *Phys. Rev. B* **84**, 195314 (2011).
- [22] C. Kloeffel, M. J. Rančić, and D. Loss, Direct Rashba spin-orbit interaction in Si and Ge nanowires with different growth directions, *Phys. Rev. B* **97**, 235422 (2018).
- [23] J.-W. Luo, S.-S. Li, and A. Zunger, Rapid transition of the hole Rashba effect from strong field dependence to saturation in semiconductor nanowires, *Phys. Rev. Lett.* **119**, 126401 (2017).

- [24] R. Li, Searching strong ‘spin’-orbit coupled one-dimensional hole gas in strong magnetic fields, *Journal of Physics: Condensed Matter* **34**, 075301 (2022).
- [25] R. Li and X.-Y. Qi, Two-band description of the strong ‘spin’-orbit coupled one-dimensional hole gas in a cylindrical Ge nanowire, *Journal of Physics: Condensed Matter*, **35**, 135302 (2023).
- [26] C. Kloeffel, M. Trif, P. Stano, and D. Loss, Circuit QED with hole-spin qubits in Ge/Si nanowire quantum dots, *Phys. Rev. B* **88**, 241405 (2013).
- [27] G. Scappucci, C. Kloeffel, F. A. Zwanenburg, D. Loss, M. Myronov, J.-J. Zhang, S. De Franceschi, G. Katsaros, and M. Veldhorst, The germanium quantum information route, *Nature Reviews Materials* **6**, 926 (2021).
- [28] C. Adelsberger, M. Benito, S. Bosco, J. Klinovaja, and D. Loss, Hole-spin qubits in Ge nanowire quantum dots: Interplay of orbital magnetic field, strain, and growth direction, *Phys. Rev. B* **105**, 075308 (2022).
- [29] K. Wang, G. Xu, F. Gao, H. Liu, R.-L. Ma, X. Zhang, Z. Wang, G. Cao, T. Wang, J.-J. Zhang, D. Culcer, X. Hu, H.-W. Jiang, H.-O. Li, G.-C. Guo, and G.-P. Guo, Ultrafast coherent control of a hole spin qubit in a germanium quantum dot, *Nature Communications* **13**, 206 (2022).
- [30] R. Li and H. Zhang, Electrical manipulation of a hole ‘spin’-orbit qubit in nanowire quantum dot: The nontrivial magnetic field effects, *Chinese Physics B*, **32**, 030308 (2023).
- [31] R. Li, Spin-photon interaction in a nanowire quantum dot with asymmetrical confining potential, *arXiv e-prints*, arXiv:2309.14693 (2023).
- [32] F. Maier, J. Klinovaja, and D. Loss, Majorana fermions in Ge/Si hole nanowires, *Phys. Rev. B* **90**, 195421 (2014).
- [33] F. K. de Vries, J. Shen, R. J. Skolasinski, M. P. Nowak, D. Varjas, L. Wang, M. Wimmer, J. Ridderbos, F. A. Zwanenburg, A. Li, S. Koelling, M. A. Verheijen, E. P. A. M. Bakkers, and L. P. Kouwenhoven, Spin-orbit interaction and induced superconductivity in a one-dimensional hole gas, *Nano Letters* **18**, 6483 (2018).
- [34] J. M. Luttinger and W. Kohn, Motion of electrons and holes in perturbed periodic fields, *Phys. Rev.* **97**, 869 (1955).
- [35] J. M. Luttinger, Quantum theory of cyclotron resonance in semiconductors: General theory, *Phys. Rev.* **102**, 1030 (1956).
- [36] N. O. Lipari and M. Altarelli, Theory of indirect excitons in semiconductors, *Phys. Rev. B* **15**, 4883 (1977).
- [37] G. Liao, N. Luo, Z. Yang, K. Chen, and H. Q. Xu, Electronic structures of [001]- and [111]-oriented InSb and GaSb free-standing nanowires, *Journal of Applied Physics* **118**, 094308 (2015).
- [38] N. Luo, G. Liao, and H. Q. Xu, k.p theory of free-standing narrow band gap semiconductor nanowires, *AIP Advances* **6**, 125109 (2016).
- [39] O. Madelung, *Semiconductors: data handbook* (Springer Science & Business Media, 2004).
- [40] D. Csontos, P. Brusheim, U. Zülicke, and H. Q. Xu, Spin- $\frac{3}{2}$ physics of semiconductor hole nanowires: Valence-band mixing and tunable interplay between bulk-material and orbital bound-state spin splittings, *Phys. Rev. B* **79**, 155323 (2009).
- [41] P. Lawaetz, Valence-band parameters in cubic semiconductors, *Phys. Rev. B* **4**, 3460 (1971).
- [42] Z. X. Wang and D. R. Guo, *Special Functions* (World Scientific, Singapore, 1989).
- [43] R. Li, Low-energy subband wave-functions and effective g-factor of one-dimensional hole gas, *Journal of Physics: Condensed Matter* **33**, 355302 (2021).
- [44] R. Li and Z.-Q. Li, Low-energy hole subband dispersions in a cylindrical Ge nanowire: the effects of the nanowire growth direction, *Journal of Physics: Condensed Matter*, **35**, 345301 (2023).
- [45] L. Wang and M. W. Wu, Hole spin relaxation in *p*-type (111) GaAs quantum wells, *Phys. Rev. B* **85**, 235308 (2012).
- [46] I. A. Kokurin, Dimensional quantization and zero-field spin splitting of holes in GaAs nanowires, *Phys. Rev. B* **108**, 165301 (2023).
- [47] L. D. Landau and E. M. Lifshitz, *Quantum Mechanics* (Pergamon, New York, 1965).
- [48] B. A. Bernevig, T. L. Hughes, and S.-C. Zhang, Quantum spin hall effect and topological phase transition in HgTe quantum wells, *Science* **314**, 1757 (2006).
- [49] X.-L. Qi and S.-C. Zhang, Topological insulators and superconductors, *Rev. Mod. Phys.* **83**, 1057 (2011).